Version of Record: https://journals.jps.jp/doi/10.7566/JPSJ.95.053601
Journal of the Physical Society of Japan, **95**, 053601 (2026). Manuscript Number: 18173, DOI: 10.7566/JPSJ.95.053601

Physically Interpretable Force Constants Based on Spherical Tensor Expansion: Efficient Parameter Reduction for Low-Symmetry Systems

Daigo Ito, Kota Hashimoto, Tomonori Tanaka, and Yoshihiro Gohda*

Department of Materials Science and Engineering, Institute of Science Tokyo, Yokohama 226-8501, Japan

Calculating interatomic force constants in disordered systems is computationally challenging due to numerous independent parameters. We propose an efficient parameter reduction methodology by transforming force constants into physically interpretable descriptors based on spherical tensor expansion. This method reveals that antisymmetric components, representing local rotational forces, are much smaller than other factors. By truncating these parameters in amorphous Si_3N_4, we reduce the number of independent fitting parameters by one-third while maintaining model accuracy. The hold-out method confirms that this physically grounded approximation accelerates training convergence while preserving the prediction accuracy of restoring forces.

Interatomic force constants (IFCs) constitute the fundamental parameters describing the potential energy surface, phase equilibria, lattice dynamics, and thermal properties of materials.[1–7] Calculating IFCs typically involves determining a vast number of independent parameters from first-principles calculations.[8–10] To make this computationally controllable, reducing the number of independent parameters is a critical and necessary step. Traditionally, this reduction heavily relies on two primary strategies: (1) defining a spatial cutoff radius beyond which interactions are deemed negligible, and (2) strictly exploiting the spatial symmetry of the crystal lattice to constrain and equate dependent elements of IFCs.[11–13] While these conventional approaches are highly successful for perfect periodic crystals,[14–22] the latter encounters severe limitations when applied to disordered systems, such as amorphous materials or crystal structures containing point defects.[23–26] In such non-symmetric environments, the lack of spatial symmetry renders the second strategy entirely ineffective.[27] Consequently, the number of independent parameters scales drastically, making calculations highly susceptible to numerical noise or the overfitting of IFCs.[28,29]

To overcome this bottleneck, an alternative approximation strategy is required: instead of relying on exact geometric symmetry, one must systematically neglect specific components of the interaction that have minimal physical impact on the overall dynamics. However, implementing such an approximation is extremely difficult with the standard Cartesian representation of IFCs, as the individual matrix elements strictly depend on the choice of the coordinate system and obscure intuitive physical meanings. To safely and effectively truncate negligible effects, it is essential to establish a force constant calculation method grounded in physical intuition.

Here, we propose a methodology to transform matrices of IFCs into physically interpretable parameters by setting the relative vector of each atomic pair as the local axis and expanding the interactions into a spherical tensor basis. By regarding these parameters as fitting parameters in the calculation of IFCs, this method can identify physically minor interactions. Thereby, we aim to perform IFCs calculations in amorphous and defective materials more effectively. To demonstrate the validity and efficiency of the proposed methodology, we systematically investigate both crystalline and amorphous phases of silicon nitride (Si_3N_4).[30–33] Our strategy is to first establish a physical baseline using perfect crystals. These amorphous materials often possess hidden local order and distinct nearest-neighbor networks similar to the perfect crystal.[34] Because directly identifying physically small interaction components in a disordered material is difficult, analyzing the components of IFCs in a stable, well-ordered environment with the proposed method allows us to identify minor interactions. This insight can provide the physical justification required to systematically truncate parameters in the complex amorphous system.

The total potential energy U of a crystal system can be expanded in terms of atomic displacements $u(l\kappa)$ from their equilibrium positions. In the harmonic approximation, this expansion is given by:

$$U \approx U_0 + \frac{1}{2}\sum_{l\kappa,l'\kappa'}\sum_{\alpha\beta}\Phi_{\alpha\beta}(l\kappa,l'\kappa')u_\alpha(l\kappa)u_\beta(l'\kappa'), \qquad (1)$$

where U_0 represents the potential energy of the equilibrium structure, l and κ denote the unit cell index and the atom index within the cell, respectively, and α,β represent the Cartesian indices (x,y,z). The coefficients $\Phi_{\alpha\beta}(l\kappa,l'\kappa')$ are the second-order IFCs, defined as the second partial derivatives of the potential energy:

$$\Phi_{\alpha\beta}(l\kappa,l'\kappa') = \frac{\partial^2 U}{\partial u_\alpha(l\kappa)\partial u_\beta(l'\kappa')}. \qquad (2)$$

For a specific atomic pair consisting of atom κ in cell l and atom κ' in cell l', we consider the 3×3 IFCs' matrix $\boldsymbol{\Phi}(l\kappa,l'\kappa')$. Let $\boldsymbol{R}$ be the relative position vector pointing from $l\kappa$ to $l'\kappa'$. We define a local coordinate system where the z-axis aligns with $\boldsymbol{R}$. The IFCs' matrix in the global Cartesian frame, $\boldsymbol{\Phi}$, is transformed into the local frame $\boldsymbol{\Phi}^{(\mathrm{loc})}$ via a rotation matrix $\boldsymbol{Q} \in \mathrm{SO}(3)$ such that $\boldsymbol{QR} = (0,0,|\boldsymbol{R}|)^\mathsf{T}$:

$$\boldsymbol{\Phi}^{(\mathrm{loc})} = \boldsymbol{Q}^\mathsf{T}\boldsymbol{\Phi}\boldsymbol{Q}. \qquad (3)$$

It should be noted that the choice of the rotation matrix $\boldsymbol{Q}$ is not uniquely determined by this condition. There remains an arbitrary degree of freedom corresponding to a spatial rotation

*Corresponding author. gohda@mct.isct.ac.jp

about the newly defined z-axis, which is aligned with the relative vector $\boldsymbol{R}$. Consequently, any rotation matrix $\boldsymbol{Q}$ satisfying this alignment condition can be chosen arbitrarily. This transformation allows us to treat the interactions in a unified local coordinate system, independent of the direction of the atomic pair in the global frame. This $\boldsymbol{\Phi}^{(\mathrm{loc})}$ is then expanded using a real spherical tensor basis $\boldsymbol{A}_m^{(l)}$, indexed by l ($l = 0, 1, 2$) and m ($-l \le m \le l$):[35]

$$\boldsymbol{\Phi}^{(\mathrm{loc})} = \sum_{l=0}^{2} \sum_{m=-l}^{l} a_m^{(l)} \boldsymbol{A}_m^{(l)}. \tag{4}$$

The expansion coefficients $a_m^{(l)}$ are mathematically determined by projecting the local IFCs'matrix onto the basis matrices. The explicit forms of the basis matrices $\boldsymbol{A}_m^{(l)}$ are defined as follows:

$l = 0$ **:**

$$\boldsymbol{A}_0^{(0)} = \frac{1}{\sqrt{3}} \begin{pmatrix} 1 & 0 & 0 \\ 0 & 1 & 0 \\ 0 & 0 & 1 \end{pmatrix}. \tag{5}$$

$l = 1$ **:**

$$\boldsymbol{A}_0^{(1)} = \frac{1}{\sqrt{2}} \begin{pmatrix} 0 & -1 & 0 \\ 1 & 0 & 0 \\ 0 & 0 & 0 \end{pmatrix},$$

$$\boldsymbol{A}_1^{(1)} = \frac{1}{\sqrt{2}} \begin{pmatrix} 0 & 0 & -1 \\ 0 & 0 & 0 \\ 1 & 0 & 0 \end{pmatrix}, \boldsymbol{A}_{-1}^{(1)} = \frac{1}{\sqrt{2}} \begin{pmatrix} 0 & 0 & 0 \\ 0 & 0 & 1 \\ 0 & -1 & 0 \end{pmatrix}. \tag{6}$$

$l = 2$ **:**

$$\boldsymbol{A}_0^{(2)} = \frac{1}{\sqrt{6}} \begin{pmatrix} -1 & 0 & 0 \\ 0 & -1 & 0 \\ 0 & 0 & 2 \end{pmatrix},$$

$$\boldsymbol{A}_1^{(2)} = \frac{1}{\sqrt{2}} \begin{pmatrix} 0 & 0 & 1 \\ 0 & 0 & 0 \\ 1 & 0 & 0 \end{pmatrix}, \boldsymbol{A}_{-1}^{(2)} = \frac{1}{\sqrt{2}} \begin{pmatrix} 0 & 0 & 0 \\ 0 & 0 & 1 \\ 0 & 1 & 0 \end{pmatrix},$$

$$\boldsymbol{A}_2^{(2)} = \frac{1}{\sqrt{2}} \begin{pmatrix} 1 & 0 & 0 \\ 0 & -1 & 0 \\ 0 & 0 & 0 \end{pmatrix}, \boldsymbol{A}_{-2}^{(2)} = \frac{1}{\sqrt{2}} \begin{pmatrix} 0 & 1 & 0 \\ 1 & 0 & 0 \\ 0 & 0 & 0 \end{pmatrix}. \tag{7}$$

The basis matrices $\boldsymbol{A}_m^{(l)}$ form an orthonormal set under the Frobenius inner product defined by $\langle \boldsymbol{A}, \boldsymbol{B} \rangle = \mathrm{Tr}(\boldsymbol{A}^{\mathsf{T}} \boldsymbol{B})$. This orthonormality is expressed as

$$\langle \boldsymbol{A}_m^{(l)}, \boldsymbol{A}_{m'}^{(l')} \rangle = \mathrm{Tr}\left[(\boldsymbol{A}_m^{(l)})^{\mathsf{T}} \boldsymbol{A}_{m'}^{(l')} \right] = \delta_{mm'} \delta_{ll'}, \tag{8}$$

where δ_{ij} is the Kronecker delta. Thanks to this property, the expansion coefficients $a_m^{(l)}$ are uniquely determined by projecting the local IFCs' matrix onto the basis matrices:

$$a_m^{(l)} = \mathrm{Tr}\left[(\boldsymbol{A}_m^{(l)})^{\mathsf{T}} \boldsymbol{\Phi}^{(\mathrm{loc})} \right]. \tag{9}$$

The physical interpretation of each coefficient is summarized below. Because $a_{\pm1}^{(1)}, a_{\pm1}^{(2)}$, and $a_{\pm2}^{(2)}$ terms are subject to rotational arbitrariness, we evaluate their norms here.

$a_0^{(0)}$**:** Generates an isotropic restoring force opposing the displacement, regardless of its direction. A more negative value indicates a stiffer isotropic spring.

$a_0^{(1)}$**:** Generates a force inducing rotation around the relative vector axis.

$a_0^{(2)}$**:** Generates restoring forces with distinct values for displacements along the relative vector and those perpendicular to it. A more negative value signifies a stiffer connection along the direction of the atomic pair.

$\sqrt{\left(a_{-1}^{(1)}\right)^2 + \left(a_1^{(1)}\right)^2}$**:** Generates a force inducing rotation around axes perpendicular to the relative vector.

$\sqrt{\left(a_{-1}^{(2)}\right)^2 + \left(a_1^{(2)}\right)^2}$**:** Generates a shear force perpendicular to the relative vector in response to a longitudinal displacement.

$\sqrt{\left(a_{-2}^{(2)}\right)^2 + \left(a_2^{(2)}\right)^2}$**:** Generates an anisotropic force in the plane perpendicular to the relative vector.

Finally, we describe the procedure to determine the IFCs. We treat the expansion coefficients $\{a_m^{(l)}\}$ as independent parameters to be optimized via the finite displacement method. Using the force–displacement relation in the harmonic approximation

$$F_\alpha(l\kappa) \approx -\sum_{l'\kappa'} \sum_{\beta} \Phi_{\alpha\beta}(l\kappa, l'\kappa') u_\beta(l'\kappa'), \tag{10}$$

and applying the inverse transformation of the spherical tensor expansion, the independent parameters $a_m^{(l)}$ are determined by minimizing the residual between the forces calculated by density functional theory (DFT)[36,37] and the model forces using the least-squares method.

We performed first-principles calculations based on DFT within the projector augmented-wave method[38] as built into the VASP code.[39,40] The exchange-correlation functional was treated within the generalized gradient approximation by Perdew, Burke and Ernzerhof.[41] A plane-wave cutoff energy of 520 eV was used throughout all structural relaxations and force calculations. For the crystalline reference, a 224-atom supercell of the stable β-Si_3N_4 phase was prepared. The amorphous Si_3N_4 model was generated via a melt-quench procedure using *ab initio* molecular dynamics.[34,42] A cubic supercell containing 112 atoms (48 Si and 64 N) was initialized with random atomic positions and a fixed lattice constant of 10.745 Å to match the macroscopic density of 3.0 g/cm^3. The molecular dynamics simulation was carried out solely at the Γ point. The system was first melted at 5000 K for 15 ps, followed by rapid quenching to 300 K at a cooling rate of 50 K/ps. Subsequently, the internal atomic coordinates were fully relaxed at the fixed cell volume, employing a $3\times3\times3$ k-point mesh and a force convergence criterion of 0.005 eV/Å. To evaluate the interatomic force constants, 150 distinct displaced configurations were generated for each phase by applying small random atomic displacements of 0.01 Å to the fully relaxed supercells. The restoring forces acting on the atoms were calculated via DFT using a $3 \times 3 \times 3$ k-point mesh and a strict electronic energy convergence criterion of 10^{-6} eV.

We first analyzed the IFCs' expansion coefficients of the crystalline β-Si_3N_4. A quantitative analysis of these expansion coefficients reveals that the antisymmetric components $l = 1$ in Figs. 1(b) and (c) are distributed within a narrower range compared to the $l = 0$ components in Fig. 1(a) and $l = 2$ components in Figs. 1(d)–(f). For instance, in the strong nearest-neighbor Si–N interactions, the value of the isotropic restoring forces $a_0^{(0)}$ reaches -12.6 eV/Å^2, and the anisotropic component $a_0^{(2)}$ reaches -9.7 eV/Å^2. In contrast, the $a_m^{(1)}$ terms

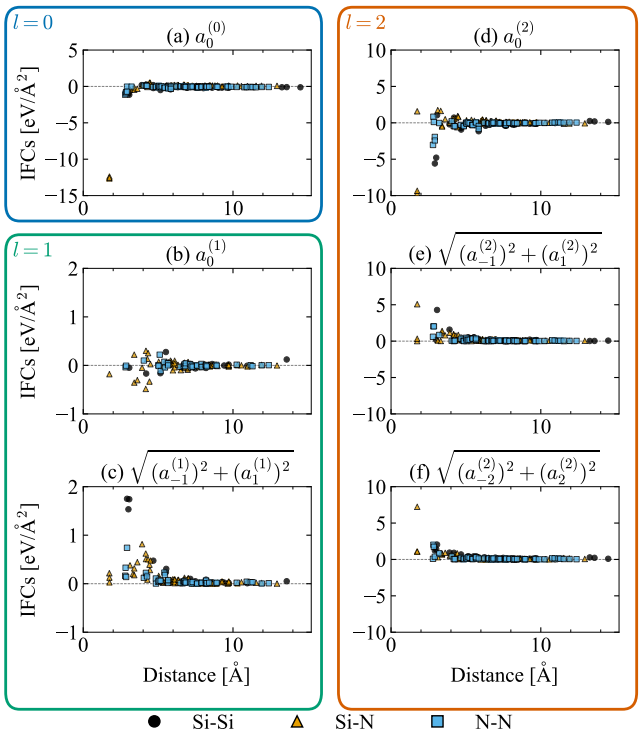

Fig. 1. (Color online) Spherical tensor expansion coefficients of the IFCs for the crystalline β-Si_3N_4 reference. The horizontal axis represents the interatomic distance, and the vertical axis represents the value of the coefficients. The data points are distinguished by color and marker shape according to the atomic pairs (circles for Si–Si, triangles for Si–N, and squares for N–N). The panels correspond to: (a) $a_0^{(0)}$, (b) $a_0^{(1)}$, (c) $\sqrt{\left(a_{-1}^{(1)}\right)^2 + \left(a_1^{(1)}\right)^2}$, (d) $a_0^{(2)}$, (e) $\sqrt{\left(a_{-1}^{(2)}\right)^2 + \left(a_1^{(2)}\right)^2}$, and (f) $\sqrt{\left(a_{-2}^{(2)}\right)^2 + \left(a_2^{(2)}\right)^2}$.

exhibit a narrow distribution, remaining around 0.2 eV/Å^2 for nearest neighbors and bounded below 1.8 eV/Å^2 overall, whereas the $a_m^{(0)}$ and $a_m^{(2)}$ terms span much broader ranges. The observed smallness of the $l = 1$ components is not accidental but is fundamentally rooted in the symmetry of interatomic interactions. The $l = 1$ components, representing the antisymmetric part of the force constant matrix, strictly vanish for any pure two-body potential depending only on the interatomic distance. In real materials, these terms emerge only as multibody effects and consistently remain smaller than the other forces derived from $l = 0$ and $l = 2$ components that govern primary stretching and bending. Leveraging this physical insight, we introduce an approximation to systematically neglect these $l = 1$ components. This simplification effectively reduces the number of independent parameters for the IFCs in complex amorphous systems without losing the essential physical characteristics of the underlying interatomic interactions.

Before applying this approximation to the amorphous phase, we verified that the local atom environment remains structurally comparable to that of the crystalline phase. Figure 2 compares the radial distribution functions (RDF) of the Si–N atomic pairs for both the crystalline and amorphous Si_3N_4 models. The first nearest-neighbor peak in the amorphous phase remains as sharp as in the crystal, centered around 1.75 Å. This indicates that the interactions in the amorphous phase exhibit similar tendencies to those in the crystal. Consequently, we can infer that the overall structure of the IFCs is broadly analogous between the two phases, suggesting that the contribution of the $l = 1$ antisymmetric components remains small in the amorphous system as well.

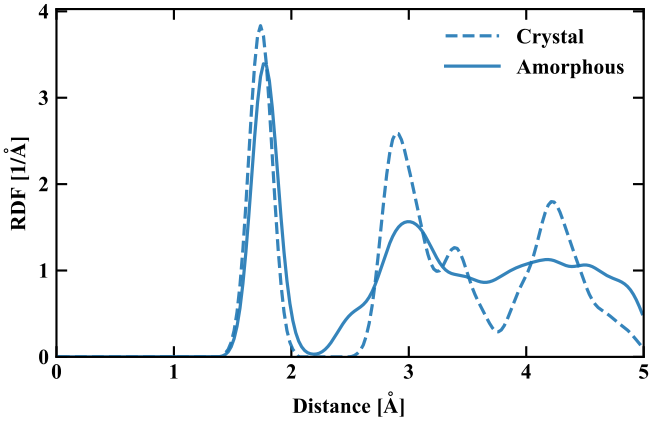

Fig. 2. (Color online) RDF of the Si–N atomic pairs for the crystalline β-Si_3N_4 (dashed line) and amorphous Si_3N_4 (solid line) structures.

Motivated by this physical justification, we applied the parameter reduction scheme to the amorphous Si_3N_4 system. In an amorphous supercell consisting of N_{atom} atoms, the absence of point group symmetry inherently leads to a massive number of independent parameters. In such disordered structures, handling all these variables is computationally demanding. By introducing a spatial cutoff radius of 4.0 Å for our supercell with $N_{\text{atom}} = 112$, the number of independent parameters for IFCs, M, is 11187. Since each displaced configuration provides $3N_{\text{atom}}$ equations, more than $M/3N_{\text{atom}}$ independent structures are theoretically required to determine the IFCs. By systematically neglecting the $l = 1$ components as mentioned previously, the number of fitting parameters further decreases by one-third to 7458. To quantitatively evaluate the validity and convergence of this approximation, we performed a validation analysis using 150 finite-displacement structures. For this evaluation, we adopted a hold-out method with a 1 : 14 split ratio; 10 structures were fixed as the test set, while the remaining 140 structures were utilized for training. Since the atomic displacements in these structures are generated randomly, this hold-out set is expected to be sufficiently representative of the configuration space. We define the prediction error (validation error) as the root-mean-square error (RMSE) between the predicted forces and the true forces obtained from DFT:

$$\text{RMSE} = \sqrt{\frac{1}{3L_{\text{test}}N_{\text{atom}}} \sum_{s=1}^{L_{\text{test}}} \sum_{n=1}^{N_{\text{atom}}} \left\| \boldsymbol{F}_{s,n}^{\text{pred}} - \boldsymbol{F}_{s,n}^{\text{true}} \right\|^2}, \qquad (11)$$

where L_{test} is the number of test structures, and $\boldsymbol{F}_{s,n}^{\text{true}}$ represents the DFT-calculated force vector acting on atom n in the s-th test structure. The corresponding predicted forces $\boldsymbol{F}_{s,n}^{\text{pred}}$ are directly computed from the fitted IFCs and the applied atomic displacements.

As shown in Fig. 3, the full model requires a minimum of 35 structures to initiate fitting, starting with a high validation error of 0.223 eV/Å and converging to 0.024 eV/Å at 140 structures. By contrast, the reduced model ($a_m^{(1)} = 0$) begins

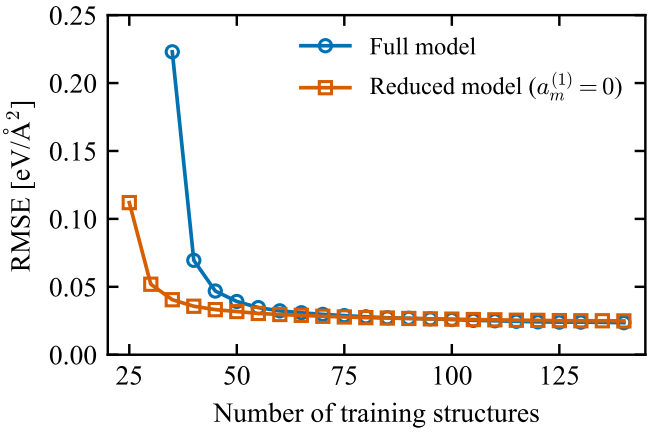

Fig. 3. (Color online) Validation error (RMSE) as a function of the number of training structures for the amorphous Si_3N_4 model. The circles represent the full model, while the squares represent the physically reduced model where the antisymmetric terms are truncated ($a_m^{(1)} = 0$).

fitting with only 25 structures due to the smaller number of parameters. Remarkably, it exhibits faster convergence, dropping to a validation error of 0.052 eV/Å with just 30 structures, and achieves a comparable accuracy of 0.025 eV/Å at 140 structures. The ultimate prediction errors of both models are nearly identical, confirming that the $l = 1$ components have little effect on the forces in the amorphous system. By systematically reducing the number of unknown parameters, the minimum required number of independent DFT calculations to initiate the fitting is effectively lowered. Therefore, this approximation method provides a highly efficient approach for calculating IFCs without compromising the fundamental dynamics of low-symmetry systems.

In summary, we developed a physics-driven parameter reduction methodology for IFCs using spherical tensor expansion. By revealing that the antisymmetric components ($l = 1$), which induce local rotation via multi-body effects, are inherently minor, we systematically truncated them in amorphous Si_3N_4. This reduced the fitting parameters by 1/3 and accelerated training convergence without compromising the predictive accuracy of restoring forces.

Looking ahead, we consider that our framework is highly compatible with data-driven parameter reduction strategies, such as sparse regression, which are widely utilized for IFCs calculations.[20,43] While standard sparse regression typically imposes a uniform penalty across all IFCs, our methodology enables more sophisticated modeling techniques by employing physically interpretable parameters for the fitting process. By assigning distinct penalties or informative priors to different groups of parameters based on their physical origins, we anticipate realizing highly efficient IFC fitting that integrates physics-driven and data-driven approaches.

Finally, our framework is extendable to higher-order anharmonic IFCs, as any n-th order IFC can be expanded using spherical tensor bases $\boldsymbol{A}_m^{(n)}$ composed of 3^n elements. While higher-order IFCs introduce greater geometrical complexity, establishing appropriate local coordinate conventions for atom clusters would ensure the physical interpretability of the expansion coefficients. Leveraging this interpretability would effectively deal with the parameter explosion in higher-order IFCs. We expect that this physics-driven method will offer an efficient pathway for exploring anharmonic lattice dynamics.

Acknowledgment This work was partly supported by MEXT-DXMag (Grant No. JPMXP1122715503) and JSPS-KAKENHI (Grant No. JP24K01144). The calculations were partly carried out by using supercomputers at ISSP, The University of Tokyo, and TSUBAME4.0, Institute of Science Tokyo.

1) R. Cowley, Adv. Phys. **12**, 421 (1963).
2) M. T. Dove, *Introduction to Lattice Dynamics* (Cambridge University Press, Cambridge, 1993) p. 64.
3) T. Tanaka and Y. Gohda, J. Phys. Soc. Jpn. **89**, 093705 (2020).
4) G. P. Srivastava, *The physics of phonons* (CRC Press, Boca Raton, 2022).
5) S. Tsuna and Y. Gohda, J. Appl. Phys. **133**, 115103 (2023).
6) S. Nishino and Y. Gohda, Jpn. J. Appl. Phys. **62**, 030902 (2023).
7) K. Hashimoto, T. Tanaka, and Y. Gohda, Phys. Rev. B **111**, 224309 (2025).
8) X. Gonze and C. Lee, Phys. Rev. B **55**, 10355 (1997).
9) K. Parlinski, Z. Li, and Y. Kawazoe, Phys. Rev. B **61**, 272 (2000).
10) S. Baroni, S. De Gironcoli, A. Dal Corso, and P. Giannozzi, Rev. Mod. Phys. **73**, 515 (2001).
11) K. Esfarjani and H. T. Stokes, Phys. Rev. B **77**, 144112 (2008).
12) A. Togo, J. Phys. Soc. Jpn. **92**, 012001 (2023).
13) A. Togo, L. Chaput, T. Tadano, and I. Tanaka, J. Phys.: Condens. Matter **35**, 353001 (2023).
14) A. A. Quong and A. Y. Liu, Phys. Rev. B **56**, 7767 (1997).
15) B. B. Karki, R. M. Wentzcovitch, S. De Gironcoli, and S. Baroni, Phys. Rev. B **61**, 8793 (2000).
16) D. A. Broido, M. Malorny, G. Birner, N. Mingo, and D. A. Stewart, Appl. Phys. Lett. **91**, 23 (2007).
17) L.-F. Huang, X.-Z. Lu, E. Tennessen, and J. M. Rondinelli, Comput. Mater. Sci. **120**, 84 (2016).
18) T. Tadano and S. Tsuneyuki, Phys. Rev. B **92**, 054301 (2015).
19) Y. Wang, Z. Lu, and X. Ruan, J. Appl. Phys. **119**, 225109 (2016).
20) T. Tadano and S. Tsuneyuki, J. Phys. Soc. Jpn. **87**, 041015 (2018).
21) Y. Oba, T. Tadano, R. Akashi, and S. Tsuneyuki, Phys. Rev. Mater. **3**, 033601 (2019).
22) R. Masuki, T. Nomoto, R. Arita, and T. Tadano, Phys. Rev. B **106**, 224104 (2022).
23) P. B. Allen and J. L. Feldman, Phys. Rev. B **48**, 12581 (1993).
24) J. L. Feldman, M. D. Kluge, P. B. Allen, and F. Wooten, Phys. Rev. B **48**, 12589 (1993).
25) J. M. Larkin and A. J. H. McGaughey, Phys. Rev. B **89**, 144303 (2014).
26) T. Wang, J. Carrete, A. van Roekeghem, N. Mingo, and G. K. Madsen, Phys. Rev. B **95**, 245304 (2017).
27) H. R. Seyf and A. Henry, J. Appl. Phys. **120**, 025101 (2016).
28) O. Hellman and I. A. Abrikosov, Phys. Rev. B **88**, 144301 (2013).
29) T. Tadano, Y. Gohda, and S. Tsuneyuki, J. Phys.: Condens. Matter **26**, 225402 (2014).
30) H. R. Philipp, J. Electrochem. Soc. **120**, 295 (1973).
31) H. Klemm, J. Am. Ceram. Soc. **93**, 1501 (2010).
32) D. J. Blumenthal, R. Heideman, D. Geuzebroek, A. Leinse, and C. Roeloffzen, Proc. IEEE **106**, 2209 (2018).
33) F. Nanataki, J.-I. Iwata, K. Chokawa, M. Araidai, A. Oshiyama, and K. Shiraishi, Jpn. J. Appl. Phys. **62**, SC1038 (2023).
34) A. Terasawa and Y. Gohda, J. Chem. Phys. **149**, 154502 (2018).
35) J. J. Sakurai, *Modern Quantum Mechanics* (Addison-Wesley, Reading, 1994) p. 232.
36) P. Hohenberg and W. Kohn, Phys. Rev. **136**, B864 (1964).
37) W. Kohn and L. J. Sham, Phys. Rev. **140**, A1133 (1965).
38) P. E. Blöchl, Phys. Rev. B **50**, 17953 (1994).
39) G. Kresse and J. Furthmüller, Comput. Mater. Sci. **6**, 15 (1996).
40) G. Kresse and J. Furthmüller, Phys. Rev. B **54**, 11169 (1996).
41) J. P. Perdew, K. Burke, and M. Ernzerhof, Phys. Rev. Lett. **77**, 3865 (1996).
42) M. D. Kluge, J. R. Ray, and A. Rahman, Phys. Rev. B **36**, 4234 (1987).
43) R. Tibshirani, J. R. Stat. Soc. Ser. B **58**, 267 (1996).